

Head on Comparison of Self- and Nano-Assemblies of Gamma Peptide Nucleic Acid Amphiphiles

Shipra Malik, Vikas Kumar, Chung-Hao Liu, Kuo-Chih Shih, Susan Krueger, Mu-Ping Nieh, and Raman Bahal*

Peptide nucleic acids (PNAs) are nucleic acid analogs with hybridization properties and enzymatic stability superior to that of DNA. In addition to gene targeting applications, PNAs have garnered significant attention as biopolymers due to the Watson–Crick-based molecular recognition and flexibility of synthesis. Here, PNA amphiphiles are engineered using chemically modified gamma PNA (8 mer in length) containing hydrophilic diethylene glycol units at the gamma position and covalently conjugated lauric acid (C12) as a hydrophobic moiety. Gamma PNA (γ PNA) amphiphiles self-assemble into spherical vesicles. Further, nano-assemblies (NA) are formulated using the amphiphilic γ PNA as a polymer via ethanol injection-based protocols. Comprehensive head-on comparison of the physicochemical and cellular uptake properties of PNA derived self- and NA is performed. Small-angle neutron and X-ray scattering analysis reveal ellipsoidal morphology of γ PNA NA that results in superior cellular delivery compare to the spherical self-assembly. Next, the functional activities of γ PNA self- and NA in lymphoma cells via multiple endpoints, including gene expression, cell viability, and apoptosis-based assays are compared. Overall, it is established that γ PNA amphiphile is a functionally active biopolymer to formulate NA for a wide range of biomedical applications.

can bind to the target DNA or RNA with high affinity and specificity via Watson–Crick base pairing.^[4] Due to the aforementioned properties, PNAs have been extensively used to target both duplex DNA^[5] and RNA^[6] for gene regulation and other diverse biomedical applications like DNA biosensing,^[7] polymerase chain reaction (PCR),^[8] diagnostics, and genomic barcoding.^[9] As compared to other nucleic acid analogs, the neutral backbone of PNA imparts it superior hybridization property toward the target DNA or RNA. However, classical PNAs are limited by numerous challenges, poor aqueous solubility, self-aggregation, non-specific interactions with macromolecules, low cellular transfection,^[10] and short in vivo elimination half-life (17 min).^[11] Hence efforts have been made to overcome the aforementioned challenges of PNAs including conjugation with cell penetrating peptides,^[12] ligands,^[13] pH low insertion peptide,^[6b] or encapsulation in nanoparticles.^[14]

PNAs have also been explored as building blocks in the field of nucleic acid nanotechnology.^[15] Until recently, peptides^[16] and DNA^[17] have been utilized for supramolecular self-assemblies (SA) with wide range of biomedical applications. However, PNAs have gained significant attention as a biopolymer, driven by the dual advantage of Watson–Crick molecular recognition of nucleic acids along with the chemical versatility and flexibility of synthesis. Several PNA modifications; conjugation with lipophilic domains,^[18] peptide motifs,^[19] combining PNAs with the self-assembled DNA units,^[20] and self-organizing guanine containing

1. Introduction

Peptide nucleic acids (PNAs), discovered three decades ago, are synthetic DNA mimics with a pseudopeptide backbone.^[1] PNAs contain repeating units of uncharged N-(2-aminoethyl) glycine units linked by amide bonds as a backbone. Nucleobases are attached via a methylene carbonyl linker to the amino nitrogen of the PNA backbone.^[2] The structural features of PNA attributes to its unique enzymatic stability while maintaining resistance to both the proteases and nucleases.^[3] Further, PNAs

S. Malik, V. Kumar, R. Bahal
Department of Pharmaceutical Sciences
University of Connecticut
Storrs, CT 06269, USA
E-mail: raman.bahal@uconn.edu
C.-H. Liu, K.-C. Shih, M.-P. Nieh
Polymer Program
Institute of Material Sciences
University of Connecticut
191 Auditorium Road, Storrs, CT 06269, USA

S. Krueger
National Institute of Standards and Technology
Gaithersburg, MD 20899-6102, USA
M.-P. Nieh
Department of Chemical and Biomolecular Engineering
University of Connecticut
Storrs, CT 06269, USA
M.-P. Nieh
Department of Biomedical Engineering
University of Connecticut
Storrs, CT 06269, USA

 The ORCID identification number(s) for the author(s) of this article can be found under <https://doi.org/10.1002/adfm.202109552>.

DOI: 10.1002/adfm.202109552

dinucleotide PNAs, also known as minimalistic PNAs,^[21] have been investigated to induce its SA into nano- or micron sized structures. In particular, PNA amphiphiles (PNAA) provide the flexible platform to assemble PNA into nanostructures for diverse biomedical applications. PNAA contain a hydrophobic domain on one end and a hydrophilic unit on the other which can be assembled into fibers, hydrogels, or micelles with tunable dimensions.^[22] Schneider et al. conjugated 12-carbon (12C) alkane tails on to the short PNA sequences containing (Lys)₂ or (Glu)₄ peptides and investigated their SA into micelles.^[14b] It was established that inclusion of 12C units does not affect the biophysical features of PNAA. Small angle X-ray scattering analysis (SAXS) of short PNA (7 nucleobase in length) conjugated with 12C units indicated formation of ellipsoidal micelles.^[23] Similarly, PNA-peptide amphiphile (PNA-PA) were formulated by conjugating a PNA sequence with small peptide sequence and alkyl chain which self-assembled into nanofibers with pH changes. PNA-PA nanofibers showed high binding affinity and specificity toward the complementary DNA and RNA targets with potential applications in gene silencing, purification, and biosensing.^[19] Another study reported SA of bilingual PNAs into micelles.^[24] These bilingual PNAs were designed by introducing hydrophilic lysine and hydrophobic alanine side chains at the gamma positions of a 12-mer PNA sequence complementary to the oncomiR-21.

The pseudopeptide backbone of PNA is amiable to chemical modifications and has been explored extensively to improve the solubility and binding affinity of PNA. Gamma modified PNAs (γ PNA) were developed by introducing a side chain at the gamma position of 2-(aminoethyl) glycine unit which induced chirality and improved binding properties contingent upon the stereochemistry.^[25] MiniPEG gamma PNA (^{MP} γ PNA) contains a diethylene glycol unit at the gamma position which introduces a (*R*)-stereogenic center resulting in pre-organization of PNA into a right-handed helical conformation.^[26] In addition to improving the recognition properties, γ PNAs also exhibit higher solubility, reduced self-aggregation, and superior biocompatibility in comparison to regular PNAs. The left and right handed (LH and RH) γ PNAs, designed by introducing different stereogenic center at the γ position, exhibit orthogonality to each other for recognition while regular PNAs, lacking any helical conformation, can bind to either of the complementary γ PNAs.^[27] This orthogonal property of LH and RH γ PNAs has been exploited to organize small PNAs with 5 nucleobases into molecular SA and was proposed as “all-in-one” platform for organization and molecular assembly.^[27] A recent study reported SA of ^{MP} γ PNAs into nano-fibers following the single stranded tile approach in DNA nanotechnology using organic solvents.^[28] These studies have established the potential of γ PNA to self-assemble into nanostructures.

In this study, we designed PNAA using short length (8mer) ^{MP} γ PNA containing the diethylene glycol units as the hydrophilic domain and lauric acid (C12 alkane) group as the hydrophobic tail. Covalent conjugation of ^{MP} γ PNA with the lauric acid results in the SA of amphiphilic PNA into nanostructures. The designed amphiphilic PNA was formulated into nano-assemblies (NA) using ethanol injection-based technique.

To investigate the functional activity, we designed a short 8mer PNA sequence complementary to the seed region

(a functional region on the 5' end from nucleotides 2 to 8) of oncomiR-155 using regular (PNA-155) and ^{MP} γ PNA monomers (γ PNA-155). OncomiRs are small 20–25 nucleotide length non-coding microRNAs or miRs that are highly upregulated in cancers.^[29] In prior work, we established that targeting the seed region of oncomiR-155 with 8mer PNAs can efficiently inhibit the tumor growth in a cell line-derived xenograft.^[6c] The inclusive physico-chemical characterization of PNA-155 and γ PNA-155 using dynamic light scattering (DLS) and electron microscopy indicated that only amphiphilic γ PNA-155 self-assembles into micelles and large vesicular structures. A head-to-head comparison of γ PNA-155 based SA and NA showed superior transfection efficiency of γ PNA-155 NA in multiple cell lines. Further, SAXS and small-angle neutron scattering analysis (SANS) confirmed the oblate ellipsoidal morphology of γ PNA-155 NA. Our results indicated the superior efficacy of γ PNA-155 NA in lymphoma cells based on a series of gene expression, cellular viability, and apoptosis-based analysis.

Overall, we established that ^{MP} γ PNA and lauric acid-based amphiphiles could be formulated into NA with superior transfection and functional activity in vitro. The proposed PNA amphiphile provides a novel platform to overcome the current challenges of limited cellular delivery and minimal efficacy of PNAs.

2. Results and Discussion

2.1. Design and Synthesis of PNA Oligomers

We synthesized two 8 mer-PNA oligomers complementary to the seed region of oncomiR-155 as reported previously.^[30] To investigate the role of diethylene glycol unit for inducing SA of PNAs, we synthesized γ PNA-155 containing diethylene glycol moieties at the gamma position of each PNA monomer while PNA-155 was synthesized using regular PNA monomers (Figure 1A). Lauric acid (C12) was conjugated as the hydrophobic scaffold to the N-terminus of both γ PNA-155 and PNA-155 using trioxo (OOO) as a flexible linker. To study cellular uptake and intra-cellular localization, carboxytetramethylrhodamine (TAMRA) dye was appended on to the C-terminus of both the PNA-155/ γ PNA-155 with trioxo as a linker (Figure 1B). PNAs were then purified using reversed-phase high performance liquid chromatography and molecular weight was confirmed using mass spectrometry analysis. Next, we examined the binding of the PNA-155 and γ PNA-155 with the miR-155 target via thermal denaturation studies. PNA-155/ γ PNA-155 was incubated with the target miR-155 at 1:1 ratio in physiological conditions. Consistent with the prior studies,^[26a] γ PNA-155 showed a higher thermal melting temperature (ΔT_m : 23 °C) than the regular PNA-155 (Figure S1, Supporting Information). Further, presence of lauric acid on the N-terminus did not interfere with the binding of PNA-155/ γ PNA-155 with the target miR-155.

Overall, we designed and synthesized lauric acid (C12) conjugated regular PNA-155 and γ PNA-155 amphiphiles to target the seed region of oncomiR-155 which is upregulated in B-cell lymphomas.^[31] Prior studies have reported SA of PNAs, however, here we designed γ PNA-155 amphiphiles by conjugating γ PNA with lauric acid (C12) and compared the self- and NA of γ PNA-155 for cellular delivery purposes.

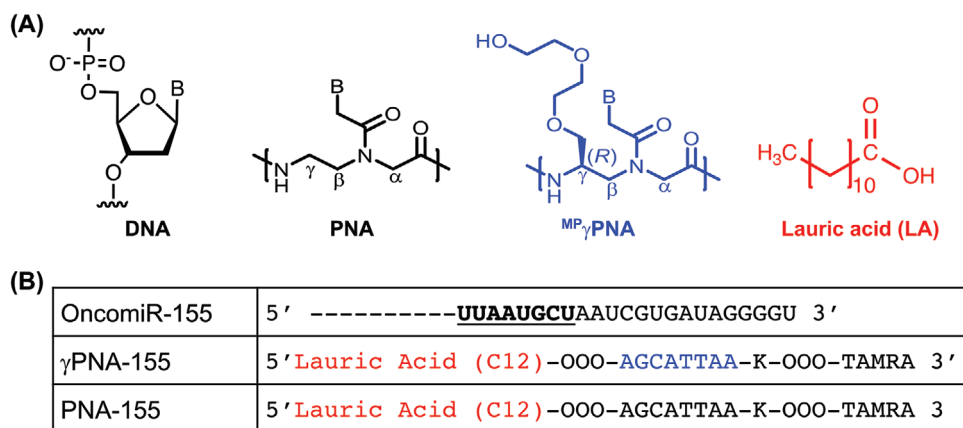


Figure 1. A) Chemical structures of DNA, PNA, MiniPEG γ PNA ($^{MP}\gamma$ PNA) monomers, and lauric acid (LA). B) The sequence of oncomiR-155 target and sequence of PNAs used in the study. The designed PNAs were complementary to the seed region of oncomiR-155 (underlined segment). γ PNA-155 was synthesized using MiniPEG γ PNA monomers and PNA-155 was synthesized using regular PNA monomers. Lauric acid was appended to N terminus or 5' end and one lysine (K) was appended to the C terminus or 3' end of both the PNAs. 5-Carboxytetramethylrhodamine (TAMRA) dye was appended to the C terminus or 3' end of both the PNAs for visualization purposes. OOO is 11-amino-3,6,9-trioxaundecanoic acid linker.

2.2. Formulation and Characterization of Self- and Nano-Assemblies

We used ethanol injection method^[32] to formulate NA using PNA-155 and γ PNA-155. The PNA-155 based nano-formulation showed significant precipitation of PNA-155 due to its hydrophobicity and poor solubility in water. Whereas, γ PNA-155 nano-formulation showed minimal signs of self-aggregation. Formulations were centrifuged to remove the aggregates and supernatant was collected for further evaluation. The concentration of nano-formulations was determined using UV–vis absorbance methods. DLS was used to determine the hydrodynamic diameter and poly dispersity index (PDI). To confirm if only PNA-155 and γ PNA-155 formed SA due to the presence of lauric acid, we also characterized the PNA-155 and γ PNA-155 dilutions in water at the same concentration as the NA. We noted that the hydrodynamic size of regular PNA-155 NA was higher (180 nm) than the only PNA-155 dilution (142 nm) in water. However, γ PNA-155 showed a significant decrease in the hydrodynamic size (100 nm) after formulation into NA in comparison to only γ PNA-155 dilution in water (>500 nm) (Figure 2A). The PDI values were less than 0.2 for the γ PNA-155 NA in comparison to the only γ PNA-155 dilutions in water. These results indicated the rearrangement of γ PNA-155 molecules into NA after formulation via ethanol injection technique (Figure 2B). We noted a change in the surface charge of PNA-155 and γ PNA-155 formulations. γ PNA-155 showed a negative zeta potential (–0.5 mV) while γ PNA-155 NA showed positive (+5 mV) surface charge density. Similarly, PNA-155 based NA showed an optimal increase in zeta potential (+20 mV) (Figure 2C).

Next, we used transmission electron microscopy (TEM) to compare the morphology of PNA-155 and γ PNA-155 based NA with the respective PNA dilutions in water. The TEM results explained that γ PNA-155 self-assembles into vesicular structures ranging from 100 to 600 nm (Figure 2D). These results are consistent with the DLS characterization of γ PNA-155 which also showed high hydrodynamic size and PDI indicating

heterogeneous distribution. The PNA-155 dilution in water showed only self-aggregation of PNA. Hence, presence of lauric acid does not induce SA of regular PNA oligomer, however conjugation of lauric acid on hydrophilic diethylene glycol modified γ PNA induces their SA into spherical vesicles. The TEM analysis of PNA-155 NA showed heterogeneous distribution of different structures ranging from micelles <100 nm to liposomal shaped structures >200 nm (Figure 2D). The major caveat of PNA-155 NA was the low concentration of supernatant after centrifugation as most of the PNA-155 is precipitated out. Hence, we further investigated only γ PNA-155 SA and NA.

2.3. Small-Angle Neutron and X-Ray Scattering Analysis

Figure 3A shows the SANS data of γ PNA-155. The oscillation at the low q possibly represents a core-shell structure. The lacking of low- q plateau suggests large radius (>1000 Å) beyond the probing q range. The attempt of using a single core-shell spherical (CSS) model (Figure S2, Supporting Information) to fit the SANS data was not successful as the best fit completely misses the high q data. It is expected since the TEM image (Figure 2B) showed two populations. The one with a smaller size should yield scattering signal at high- q range. Moreover, the SANS data of γ PNA-155 NA (Figure 3B) indicate a similar feature (for $q > 0.06 \text{ \AA}^{-1}$), suggesting both assemblies may contain similar types of smaller-sized particles. To characterize the smaller-sized vesicles, SAXS was applied to the sample because the highest probing q value extends to $q = 1.0 \text{ \AA}^{-1}$. Figure 3C shows the SAXS data of γ PNA-155 NA. A clear intensity shoulder is observed at $q \approx 0.3 \text{ \AA}^{-1}$, which cannot be clearly resolved in SANS, resembling the scattering feature of a core-shell spheres. Therefore, we applied another CSS model to best fit the SAXS data and were able to describe the data of $q > 0.05 \text{ \AA}^{-1}$ (as shown in dark dashed line in Figure 3C). The low- q mismatch is due to larger-size particles from NA. The smaller particles are presumably micelles with a best fitting

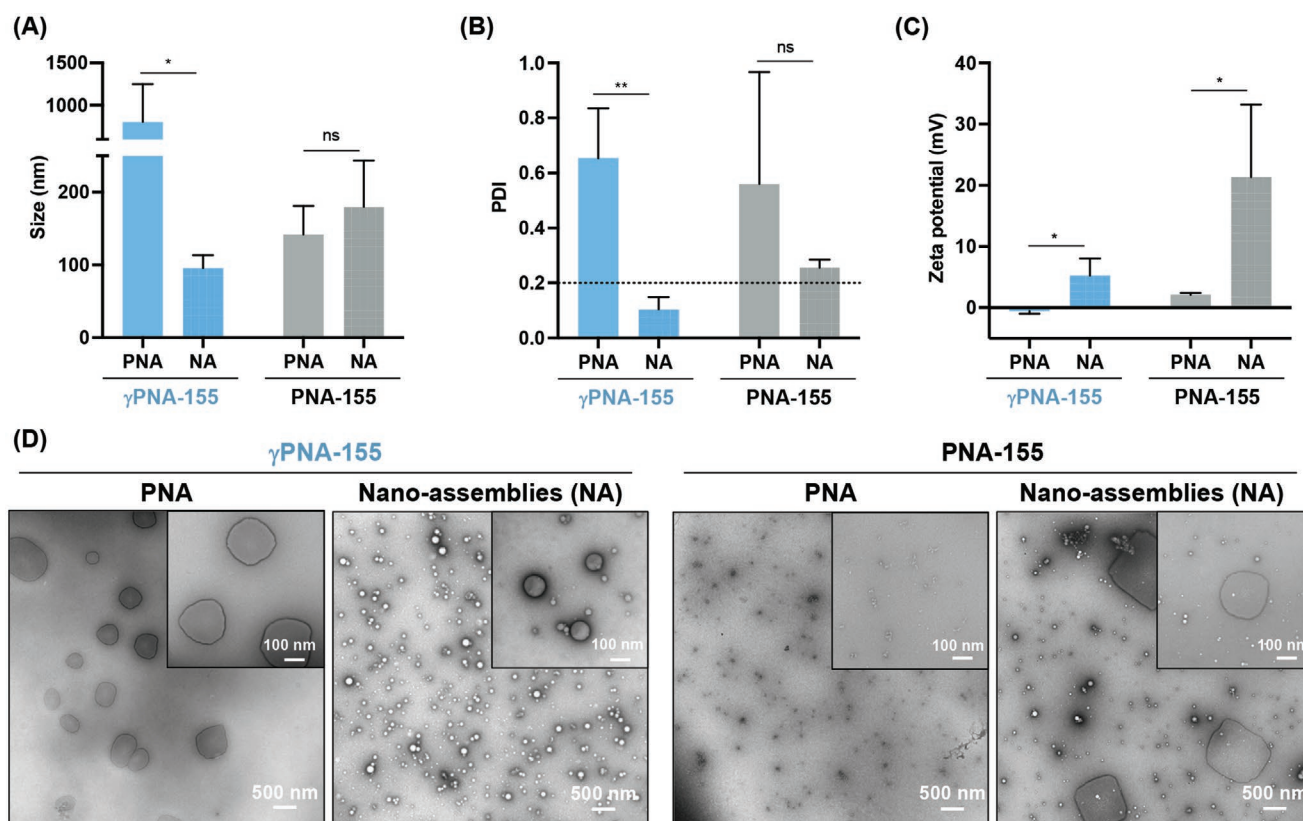


Figure 2. A) The hydrodynamic diameter, B) polydispersity index (PDI), and C) surface charge of γ PNA-155, γ PNA-155 nano-assemblies (NA), PNA-155, and PNA-155 NA. The results are presented as mean \pm SD ($n = 3$). The 10 \times dilution of γ PNA-155 NA and PNA-155 NA was used for characterization. γ PNA-155 and PNA-155 dilutions were prepared at the same concentration as the 10 \times dilutions of their respective NAs. D) Transmission electron microscopy (TEM) images of γ PNA-155, γ PNA-155 NA, PNA-155, and PNA-155 NA.

radius of 13 (± 1) Å and shell thickness of 10 (± 1) Å (Figure 3E). The structural dimensions of the micelles were then directly applied to describe the SANS data over the high- q range. As for the larger particles of the γ PNA-155 NA, (Figure 3B) the low- q intensity approaches plateau, suggesting that the dimension is smaller than of the SA. A core-shell ellipsoidal model shown in Figure 3D and Figure S2, (Supporting Information) provides a reasonable fit for the SANS data. The half lengths along the long- and short- axes of the inner water core are a and b , and the shell thicknesses along the corresponding axes are represented as d and c , respectively. Note that the rotating axis is the short one (b axis), forming an oblate-shell morphology. The best fitting structure yields an oblate shell and the dimension of its equator radius [≈ 530 (± 23) Å] agrees with the TEM images (Figure 2B) with a shorter polar radius of 43 (± 2) Å. The same dimension of the oblate structures was directly applied to the analysis of SAXS data (Figure 3C) to match the low- q initial intensity decay (the orange dashed line); however, the dimension of large particles cannot be obtained due to the inaccessible lower q range. The SANS data of γ PNA-155 can be best fit by two CSS models of different sizes. The similar structural parameters of smaller-sized particle from the γ PNA-155 NA were applied to the SANS data of γ PNA-155 because of the similar scattering pattern over the high- q range. The sum of the smaller-sized CSS model (accounting for micelles) and

another CSS model with larger size (accounting for vesicles) was applied to fit the whole range of SANS data (Figure 3A), yielding a shell thickness of 45 (± 16) Å and a vesicular radius > 1000 Å (Figure 3E). Compared to the TEM image of the γ PNA-155, which shows a wide size distribution of layered structure (100–600 nm), we presume that the planar layers are the shells of the large vesicles. As a result, the combination of SANS and SAXS data allows us to access the structures of both particles which are consistent with the TEM images because of their different probing q ranges.

2.4. Binding and Stability Study of γ PNA-155 NA

First, we examined the binding of only γ PNA-155 and γ PNA-155 NA with the miR-155 target containing predicted binding sites by gel-shift assay. We tested different ratios of γ PNA-155 with miR-155 from 1:1 to 4:1. We noted significant bound fraction ($>20\%$) of γ PNA: miR-155 heteroduplex with γ PNA-155 and γ PNA-155 NA at 1:1 ratio. The fraction of γ PNA: miR-155 heteroduplex increased with higher γ PNA-155 content (Figure S4, Supporting Information). We observed $>90\%$ binding at 4:1 ratio of γ PNA-155 and miR-155 for both the γ PNA-155 and γ PNA-155 NA. Hence, the formulation of γ PNA-155 into the NA did not impact its binding affinity with miR-155 target site.

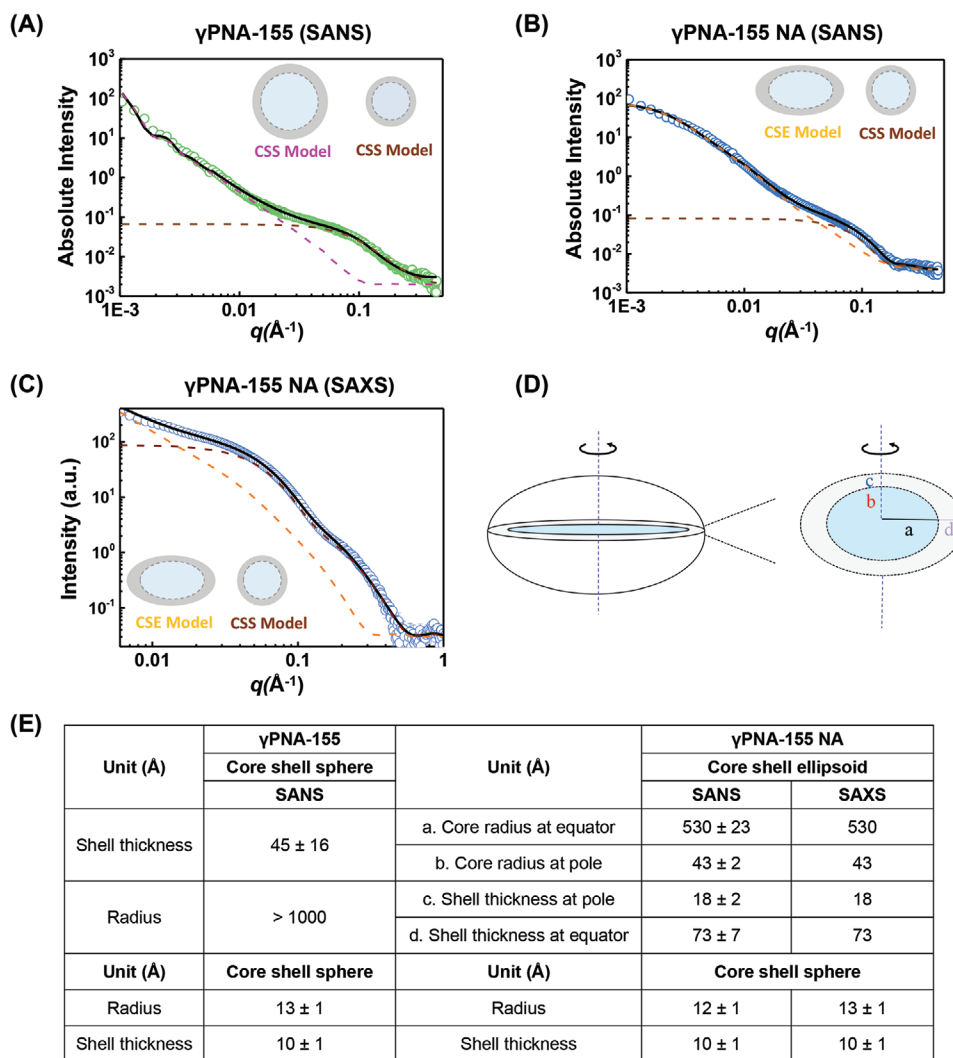


Figure 3. The SANS patterns of A) γ PNA-155 and B) γ PNA-155 NA. C) The SAXS pattern of γ PNA-155 NA. D) The cross section of the oblate ellipsoid shape of γ PNA-155 NA. E) The fitting results of γ PNA-155 (SANS) and γ PNA-155 NA (SANS and SAXS). The lighter and darker dashed lines correspond to the contributions of the larger and smaller morphologies, respectively.

Next, we evaluated the stability of γ PNA-155 NA at refrigerated conditions (4 °C) to avoid the impact of freeze-thaw cycles on the γ PNA-155 NA stability. We performed DLS to measure the changes in hydrodynamic size and PDI of the samples at regular interval of 2 days for a period of 2 weeks which was then followed by weekly measurements. We did not notice any change in the hydrodynamic size of γ PNA-155 NA over the period of the stability study. However, we noted an increase in PDI (>0.2) after 28 days (Figure S5, Supporting Information). Hence, the γ PNA-155 NA were stable for a month when stored under refrigerated conditions. We also tested the impact of ultrafiltration and lyophilization, processes routinely employed during the processing of nano-formulations, on the stability of γ PNA-155 NA. The ultrafiltration technique is used for separation, concentration, as well as quantification of encapsulation efficiency of liposomes.^[33] Similarly, lyophilization is critical to ensure the long-term stability of nano-formulations.^[34] We measured the DLS size, PDI, and the surface charge of the γ PNA-155 NA both

pre- and post-ultrafiltration and -lyophilization. We observed aggregation of γ PNA-155 NA when reconstituted after lyophilization as indicated by the increase in DLS size, PDI, and zeta potential (Figure S6, Supporting Information). These results are consistent with aggregation of nanoparticles observed after lyophilization in the absence of cryoprotectants.^[35] However, ultrafiltration showed the minimal impact on the physicochemical characteristics of γ PNA-155 NA (Figure S5, Supporting Information). Hence, ultra-filtration can be used to concentrate the γ PNA-155 NA while maintaining their characteristics.

2.5. γ PNA-155 NA Exhibit Superior Cellular Uptake

The cellular uptake of γ PNA-155 and γ PNA-155 NA was studied in two cell lines including HeLa, a cervical cancer cell line, and U2932, a B-cell lymphoma cell line to establish the potential for targeting diverse cancer cells. The uptake of both the

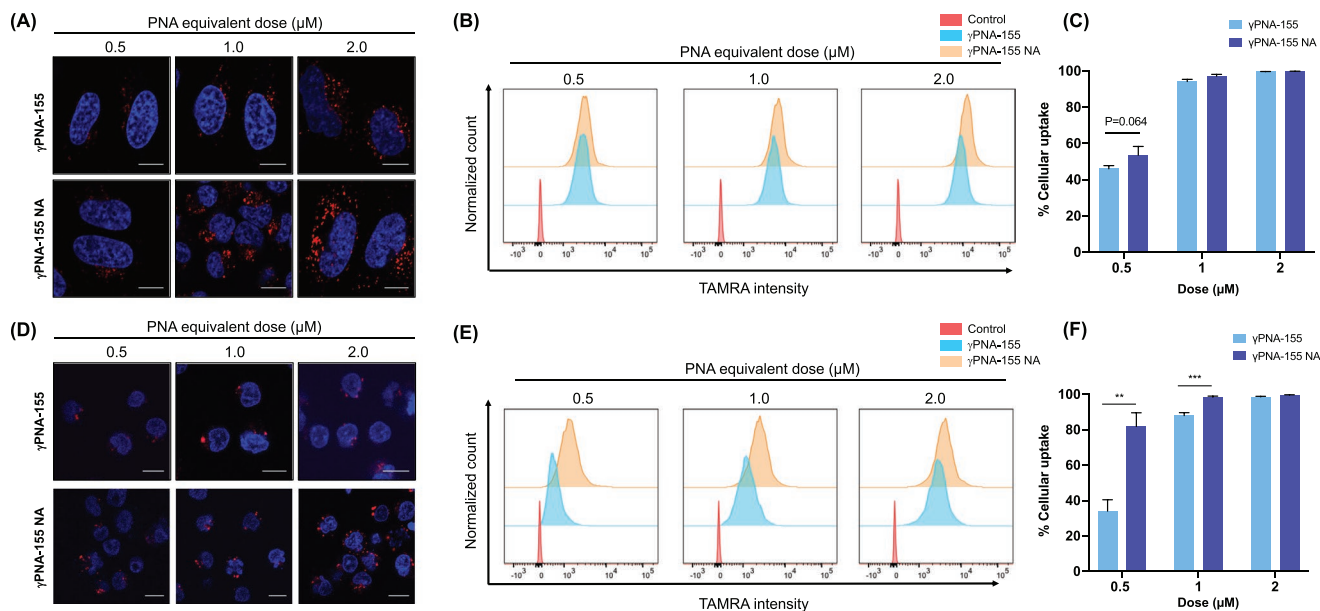


Figure 4. A) Confocal microscopy images of live HeLa cells indicating uptake of γ PNA-155 and γ PNA-155 nano-assemblies (NA) at different PNA equivalent dose after 24 h of treatment. The scale bar represents 80 pixels. Blue indicates nucleus and red indicates TAMRA. B) The flow cytometry histograms showing uptake of γ PNA-155 and γ PNA-155 NA. C) The quantification γ PNA-155 and γ PNA-155 NA containing HeLa cells at indicated doses via flow cytometry. The results are presented as mean \pm SD ($n = 3$) and t -test was used for statistical analysis. D) Confocal microscopy images of live U2932 cells after 24 h of treatment with γ PNA-155 and γ PNA-155 NA at different PNA equivalent doses. The scale bar represents 80 pixels. Blue represents nucleus and red is TAMRA. E) Flow cytometry histograms depicting the uptake of γ PNA-155 and γ PNA-155 NA in U2932 cells after 24 h of treatment. F) The quantitative representation of γ PNA-155 and γ PNA-155 NA containing U2932 cells. The results are represented as mean \pm SD ($n = 3$) and t -test was used for statistical analysis. ** $p < 0.01$, *** $p < 0.001$.

γ PNA-155 and γ PNA-155 NA was visualized via confocal microscopy and quantified using flow cytometry analysis. HeLa and U2932 cells were incubated with γ PNA-155 and γ PNA-155 NA at the same PNA equivalent dose of 0.5, 1, and 2 μ M for 24 h. We noted dose dependent increase in the cellular transfection of γ PNA-155 and γ PNA-155 NA in HeLa cells (Figure 4A). Since γ PNA-155 self-assembles into large heterogeneous structures (100–600 nm), we observed reduced cellular uptake in comparison to the γ PNA-155 NA. Confocal microscopy images of live HeLa cells showed higher TAMRA intensity in γ PNA-155 NA treated cells in comparison to only γ PNA-155 particularly at 0.5 and 1 μ M (Figure 4A). The flow cytometry analysis indicated superior transfection of γ PNA-155 NA in HeLa cells at 0.5 μ M dose (Figure 4B,C; Figure S7, Supporting Information).

Interestingly, we noted higher uptake of γ PNA-155 NA in U2932 lymphoma cells in comparison to the HeLa cells in particular at lower concentration. The differential uptake pattern of PNAs has been reported in different cell lines especially adherent and suspended cells.^[36] We observed higher cellular accumulation of γ PNA-155 NA than γ PNA-155 at 0.5 μ M PNA equivalent dose via both confocal and flow cytometry (Figure 4D,E). Flow cytometry results showed more than two-fold higher cellular uptake of γ PNA-155 NA than γ PNA-155 in U2932 cells. However, the fold change in uptake of γ PNA-155 NA in comparison to γ PNA-155 reduced with increase in the dose (Figure 4E; Figure S8, Supporting Information). Receptor mediated endocytosis has been reported to undergo saturation leading to reduced uptake at higher concentrations.^[37] Hence, the low dose treatment of γ PNA-155 NA can attain

superior therapeutic efficacy in the cancer cells in comparison to the only γ PNA-155. In addition, saturation of uptake at high dose indicates endocytosis as possible mechanism for cellular transport of γ PNA-155 and γ PNA-155 NA. Further, we correlated the structure of γ PNA-155 NA and SA with their cellular uptake. Note that both γ PNA-155 NA and SA have similar small micelles; therefore the distinct cellular uptake is likely attributed to the larger-size particles. We hypothesize that small oblate morphology of γ PNA-155 NA enhances the cellular uptake compared to the large spherical vesicles noted in the SA of γ PNA-155. This hypothesis is consistent with previous reports on the enhanced cellular uptake of lipid nanodisc (or bicelle) in contrast to spherical lipid vesicles made of the same compositions.^[6d,38] The positive charge density of γ PNA-155 NA also plays a role in the enhancement of cellular uptake.

2.6. Uptake Mechanism of γ PNA-155 and γ PNA-155 NA

Next, we investigated the uptake mechanism of γ PNA-155 and γ PNA-155 NA in the adherent HeLa cells which are widely used for the mechanistic endocytic studies. To ascertain the endocytosis role in cellular uptake of γ PNA-155 based SA and NA, we compared their transfection efficiency at low (4 $^{\circ}$ C) and physiological temperature (37 $^{\circ}$ C). It is well known that the production of ATP is reduced at 4 $^{\circ}$ C resulting in the inhibition of endocytosis-based transport across the cell membranes.^[39] Hence, we treated HeLa cells with 1 μ M equivalent dose of γ PNA-155 and γ PNA-155 NA at 37 and 4 $^{\circ}$ C for 2 h and used

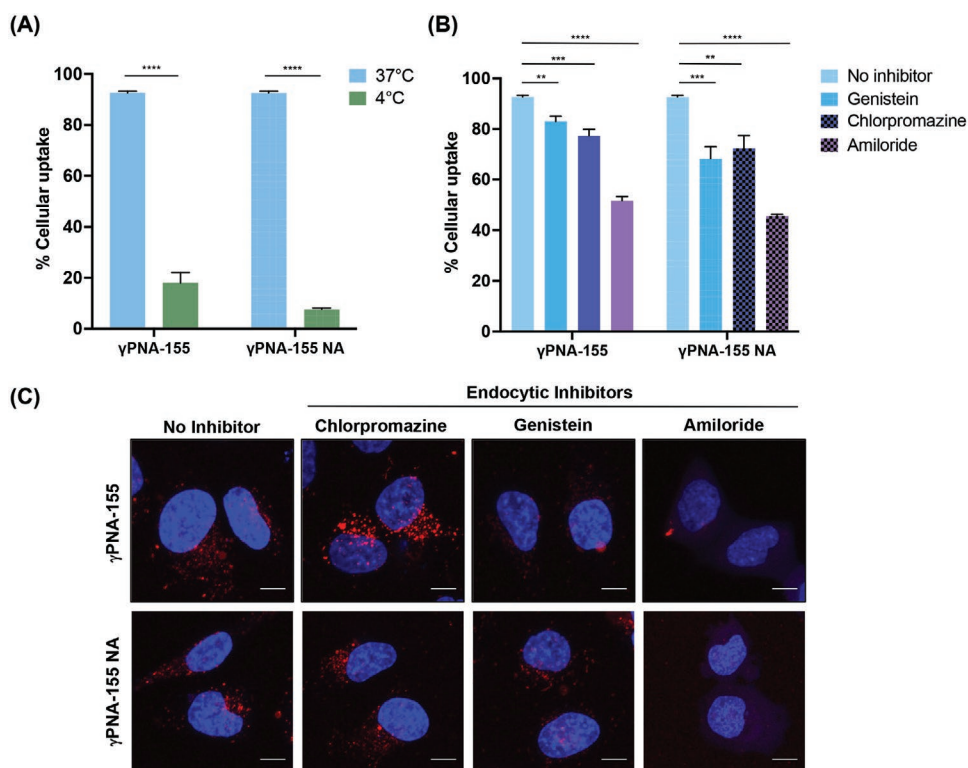


Figure 5. A) The quantitative representation of γ PNA-155 and γ PNA-155 nano-assemblies (NA) uptake in HeLa cells at 37 and 4 °C after 2 h of incubation. The results are represented as mean \pm SD ($n = 3$) and t -test was used for statistical analysis. **** $p < 0.0001$. B) Graph representing the change in cellular transport of γ PNA-155 and γ PNA-155 NA in HeLa cells via flow cytometry analysis after inhibition of endocytic pathways using genistein, chlorpromazine, and amiloride which inhibits caveolae-mediated, clathrin-mediated, and macropinocytosis cellular transport, respectively. The results are represented as mean \pm SD ($n = 3$) and t -test was used for statistical analysis. ** $p < 0.01$, *** $p < 0.001$, **** $p < 0.0001$. C) The fluorescent images of HeLa cells showing uptake of γ PNA-155 and γ PNA-155 NA after small molecule (chlorpromazine, genistein, and amiloride) mediated inhibition of endocytic pathways and 2 h treatment duration. Scale bar represents 80 pixels. Blue indicates nucleus and red is TAMRA.

flow cytometry to quantify the uptake. γ PNA-155 and γ PNA-155 NA (Figure 5A) showed a decline in uptake at 4 °C in HeLa cells. γ PNA-155 showed 80% decrease in the cellular uptake while the transfection efficiency of γ PNA-155 NA decreased more than 90%. Aforementioned results confirmed that the endocytosis-based pathways contribute toward the uptake of γ PNA-155 and γ PNA-155 NA. Further, we also investigated the contribution of different endocytic transport pathways for cellular delivery of γ PNA-155 and γ PNA-155 NA. We performed uptake studies in the presence of endocytic pathway inhibitors for mechanistic understanding of the routes for cellular transport of γ PNA-155 and γ PNA-155 NA in HeLa cells. Prior studies established that chlorpromazine (CPZ) inhibits clathrin mediated endocytic pathway,^[40] genistein prevents the caveolae based pathway,^[41] and amiloride interferes with the macropinocytosis based transport.^[42] We pre-incubated HeLa cells in the presence of different endocytic inhibitors for 1 h followed by treatment with γ PNA-155 and γ PNA-155 NA.

Further, we examined the cellular uptake via flow cytometry and confocal microscopy-based techniques. Flow cytometry results indicated the substantial role of macropinocytosis in transport of γ PNA-155 and γ PNA-155 NA (Figure 5B). Whereas, γ PNA-155 NA also undergoes uptake via clathrin and caveolae-mediated pathways. CPZ and genistein-mediated inhibition of clathrin and caveolae endocytic pathways, respectively in HeLa

cells resulted in 30% lower cellular internalization of γ PNA-155 NA. Overall, our results indicated that γ PNA-155 NA undergoes uptake via three major endocytic pathways including macropinocytosis, being the dominant route, and followed by caveolae and clathrin mediated transport. We confirmed our results by confocal imaging where we noted maximum reduction in cellular uptake of γ PNA-155 NA after amiloride mediated inhibition of macropinocytosis (Figure 5C). However, HeLa cells treated with only γ PNA-155 showed 50% reduced uptake after inhibition of macropinocytosis and less than 25% decrease in uptake after inhibition of caveolae or clathrin mediated pathways. These results are consistent with previous report, where peptide conjugated PNAs utilized macropinocytosis, clathrin, and caveolae mediated pathways for cellular transport.^[43] For the future studies, it will be interesting to combine the different endocytic pathway inhibitors and study their cumulative effect on internalization of γ PNA-155 and γ PNA-155 NA.

2.7. Safety and Efficacy Evaluation of γ PNA-155 and γ PNA-155 NA

The nucleic acids (DNA or RNA)^[44] as well as lipid nanoparticles containing positively charged lipids^[45] have been reported to activate the toll-like receptor mediated immune response.

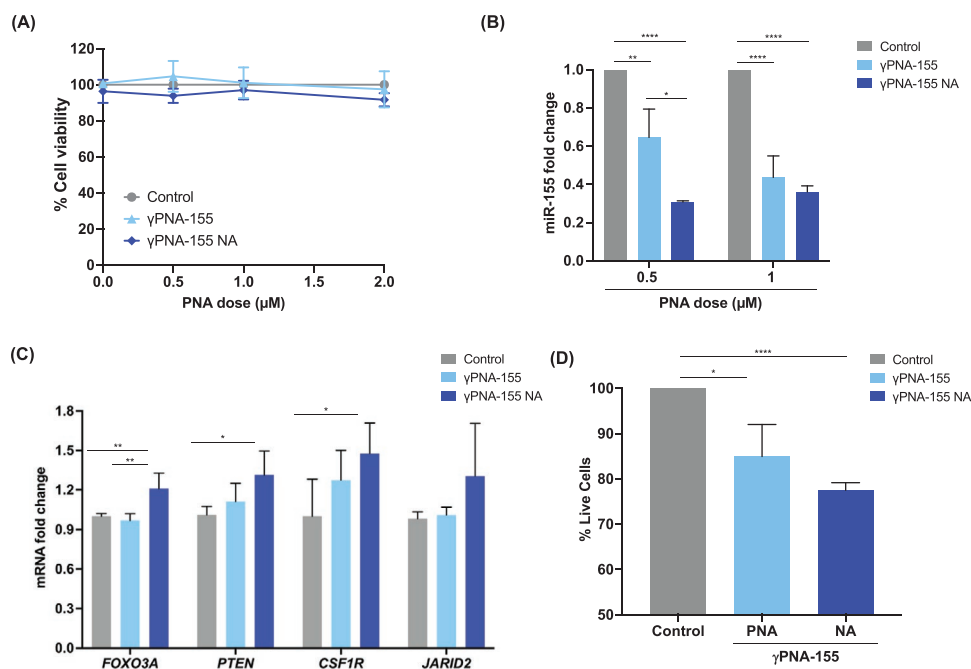


Figure 6. A) The graph representing cellular viability of peripheral blood mononuclear cells (PBMC) after 48-h treatment with γ PNA-155 and γ PNA-155 nano-assemblies (NA). Untreated cells were used as control. Results are presented as mean \pm SD ($n = 5$). B) The fold change in U2932 miR-155 levels after 48-h treatment with γ PNA-155 and γ PNA-155 NA at indicated doses. The results are presented as mean \pm SD ($n = 3$) and t -test was used for statistical analysis. * $p < 0.05$, ** $p < 0.01$, **** $p < 0.0001$. C) The fold change in levels of downstream targets of miR-155 in U2932 cells after 48-h treatment with γ PNA-155 and γ PNA-155 NA at 0.5 μ M dose. The results are presented as mean \pm SD ($n = 3$) and t -test was used for statistical analysis. * $p < 0.05$, ** $p < 0.01$. D) The change in percentage of live U2932 cells after treatment with γ PNA-155 and γ PNA-155 NA at 0.5 μ M PNA equivalent dose. The results are presented as mean \pm SD ($n = 3$) and t -test was used for statistical analysis. * $p < 0.05$, **** $p < 0.0001$.

Peripheral blood mononuclear cells (PBMC) consists of heterogeneous cell population including lymphocytes, monocytes, and macrophages which are critical components of innate and adaptive immune response.^[46] Hence, we tested the safety of γ PNA-155 and γ PNA-155 NA in PBMC in vitro. We treated the PBMC cells with increasing doses of γ PNA-155 and γ PNA-155 NA at the PNA equivalent doses of 0.5, 1, and 2 μ M. We measured the viability of PBMC cells after 48 h of treatment via luminescence-based assay. The results showed no impact of γ PNA-155 NA on the viability of PBMC cells in comparison to the control and γ PNA-155 treated cells at all indicated doses (Figure 6A).

γ PNA-155 was designed to target the seed region of oncomiR-155, which is highly overexpressed in diffuse large B cell lymphoma (DLBCL)^[47] and burkitt lymphoma.^[48] Hence, we tested the efficacy of γ PNA-155 NA in U2932 cells, a DLBCL cell line which overexpresses the oncomiR-155 in comparison to the non-tumor reactive lymph nodes.^[47] Since γ PNA-155 NA showed superior cellular transfection at low doses (0.5 and 1 μ M), we treated U2932 cells with both the γ PNA-155 and γ PNA-155 NA at two PNA equivalent doses including 0.5 and 1 μ M. Quantitative real time polymerase chain reaction (qRT-PCR) results indicated 70% knockdown of miR-155 after treatment with γ PNA-155 NA at 0.5 μ M dose in comparison to the control group (Figure 6B). However, we noted only 35% and 60% knockdown of miR-155 in γ PNA-155 treated U2932 cells at 0.5 and 1 μ M dose, respectively (Figure 6B). γ PNA-155 NA reached maximum knockdown (70%) of the target miR-155 at 0.5 μ M as we did not observe an increase in knockdown efficiency of miR-155 at 1 μ M. These observations

are consistent with the reports where receptor mediated endocytosis plays a major role for cellular transport at lower doses and is saturated at higher doses.^[49] However, only γ PNA-155 showed a dose dependent increase in the cellular delivery as well as the knockdown efficiency. These results further establish that only γ PNA-155 utilizes macropinocytosis as the major cellular uptake pathway which is not saturated at the tested concentration (0.5 and 1 μ M).

Further, we evaluated the levels of tumor suppressor genes using γ PNA-155 and γ PNA-155 NA at 0.5 μ M equivalent dose in U2932 cells. The level of genes including forkhead box O3 (FOXO3A), phosphatase and tensin homolog (PTEN), colony stimulator factor-1 receptor (CSF1R), and jumoni- and AT-rich interactive domain 2 (JARID2) have been reported to be upregulated after knockdown of miR-155 in multiple diffuse large B-cell lymphoma cell lines.^[50] We observed higher upregulation of FOXO3A, PTEN, CSF1R, and JARID2 in γ PNA-155 NA treated U2932 cells in comparison to only γ PNA-155 (Figure 6C). These results are consistent with the uptake study of γ PNA-155 NA in U2932 where we noted more than two-fold higher uptake of γ PNA-155 NA (82%) at 0.5 μ M when compared against γ PNA-155 (32%) via flow cytometry analysis. Hence, the qRT-PCR results corroborate our observations in cellular uptake studies, establishing that superior transfection properties of γ PNA-155 NA results in higher knockdown efficiency of miR-155 in comparison to γ PNA-155 at 0.5 μ M.

The high levels of oncomiR-155 are critical for the proliferation of lymphoma cells.^[51] Hence, we investigated the impact of miR-155 knockdown on U2932 cell viability. We used luminescence-

based assay to determine the viability of U2932 cells after 48 h of treatment with γ PNA-155 and γ PNA-155 NA at the PNA equivalent doses of 0.5, 1, 2, and 4 μ M. We observed significant decline in the viability of γ PNA-155 NA treated U2932 cells in comparison to the only γ PNA-155 when tested at the same dose (0.5, 1, 2, and 4 μ M) (Figure S9, Supporting Information). These results further support that γ PNA-155 NA mediated superior knockdown of oncomiR-155 results in the reduced viability of U2932 cells in comparison to γ PNA-155 treated cells. Next, we performed annexin V assay to study the role of γ PNA-155 NA mediated apoptosis in the U2932 cells. Consistent with the cellular viability studies, we observed 25% decrease in the live U2932 cells after 48 h of treatment with γ PNA-155 NA, while γ PNA-155 treated U2932 cells showed only 15% decrease in live cells when compared against the untreated cells (Figure 6D). Further, annexin V assay results showed that U2932 cells undergo early or late apoptosis after treatment with γ PNA-155 and γ PNA-155 NA. We observed higher percentage increase of apoptotic cells (22%) in γ PNA-155 NA treated U2932 cells in comparison to only γ PNA-155 (15%) treated cells at the PNA equivalent dose of 0.5 μ M (Figure S10, Supporting Information). The results from apoptosis and cell viability study together with the miR-155 knockdown in U2932 cells confirmed the higher efficacy of γ PNA-155 NA in comparison to γ PNA-155 in vitro.

3. Conclusion

The cellular delivery of PNAs has been a major challenge toward their clinical success. Until now the focus has been on utilizing nanoparticles,^[52] peptide based approaches^[53] or liposomes for improving the cellular delivery of PNAs. Here we developed a simple approach based upon nucleic acid nanotechnology to improve the cellular transport of PNAs. The superior efficacy of chemically modified γ PNAs containing diethylene glycol units have been established in multiple studies in vivo for both gene targeting^[54] and gene editing^[5a,c] applications. Most recently, few studies have also reported SA of γ PNAs containing diethylene glycol side-chains into nanofibers^[55] or complex nanostructures.^[28,56] However, in this study we designed amphiphilic γ PNAs which can be formulated into NA with superior cellular transfection and functional properties. Hence, this strategy opens a new avenue for γ PNA mediated gene targeting applications where γ PNAs can be delivered without the need of a carrier system. It would be interesting to deliver multiple PNA sequences formulated into NA to target different RNA (coding or non-coding) for treating cancer and metabolic disorders. It would also be interesting to study the stability, safety, and efficacy of these amphiphilic γ PNA based NA in vivo.

Overall, we established that amphiphilic γ PNAs can be successfully formulated into NA which exhibit superior cellular transfection and functional activity in vitro. We exploited the potential of γ PNA as a biopolymer to formulate biologically active NA using a simple and easily scalable approach. Unlike DNA, PNAs are enzymatically stable and non-immunogenic, hence PNA based NA can be utilized for diverse biomedical applications. This study provides the evidence that PNAs can be engineered as the compatible biomaterial to design the next generation of functionally active nanostructures.

4. Experimental Section

Materials: The boc protected regular and mini-PEG γ PNA monomers (A, T, C, and G) were purchased from ASM Chemicals (Germany). Lauric acid and Boc-Mini-PEG-3 linker was obtained from Sigma Aldrich (USA). TAMRA or carboxytetramethylrhodamine dye was obtained from VWR International. Fmoc-Lysine (Boc)-OH was purchased from Sigma Aldrich (USA) and 4-methylbenzhydrylamine (MBHA) resin (100–200 mesh) was obtained from Peptide International (USA). The cells used in the study including HeLa (ATCC CCL-2) and PBMC were obtained from American type culture collection (ATCC, USA). U2932 cells were purchased from DSMZ (ACC-633, Germany). Eagle's minimum essential medium (EMEM, 30-2003), Roswell park memorial institute medium (RPMI-1640, 30-2001), and fetal bovine serum (FBS, 30-2020) were also bought from ATCC (USA).

Synthesis of PNA Oligomer: Fmoc-Lysine (Boc) was conjugated to the MBHA resin to use as a solid support for PNA synthesis. Boc-protected regular and Mini-PEG γ PNA monomers (A, T, C, and G) were then added to the Fmoc-Lysine (Boc) conjugated resin using solid phase synthesis as reported previously.^[30b] Lauric acid was conjugated at the N terminus of PNAs using Mini-PEG-3 as a linker. Further TAMRA was conjugated to the C terminus of PNAs also using Mini-PEG-3 as a linker. The cocktail containing trifluoroacetic acid:trifluoromethanesulfonic acid:thioanisole:m-cresol was used at 6:2:1:1 ratio to cleave the PNA oligomers from the resin. Next, diethylether was used to precipitate PNA from the cleavage cocktail and was washed twice with diethyl ether. PNAs were then vacuum dried overnight and reconstituted in acetonitrile and water. The purification of PNAs was performed using reverse phase high performance liquid chromatography (RP-HPLC, Shimadzu, Japan) and an XBridge C18 OBD prep column (Waters, USA). 0.1% v/v TFA in acetonitrile was used as the organic phase and 0.1% v/v TFA in water as the aqueous mobile phase. The pure fraction of PNAs was then freeze-dried (Labconco, USA) and reconstituted in water. The PNA concentration was determined via UV-vis spectroscopy on a Nanodrop (Thermo Scientific, USA) and was stored at -20 °C. Further the molecular weight of PNAs was confirmed using matrix assisted laser desorption-ionization time of flight spectrometry.

Formulation of PNA Nano-Assemblies: The NA were formulated using ethanol injection method as reported previously for liposome formulation.^[32] Both the PNA-155 and γ PNA-155 containing lauric acid (50 nmoles) were completely dissolved in 0.5 mL ethanol and added dropwise to the 5 mL aqueous phase (0.2 micron filtered purified water) using a 28-gauge syringe. The aqueous phase was continuously stirred at 700 RPM ($\times 0.016667$ Hz) while maintaining a temperature of 75 °C. After the addition of PNA to the aqueous phase, it was covered with aluminum foil and allowed to stir overnight at room temperature (RT) inside the chemical hood. The formulation was then centrifuged at 15 000 RPM for 10 min at 4 °C to remove the large aggregates. The supernatant was collected in a separate sterile tube and stored in 4 °C protected from light for further evaluation.

Gel Shift: γ PNA-155 and γ PNA-155 NA were incubated with the miR-155 target at indicated ratios of PNA:miR-155 ranging from 1:1 to 4:1. Samples were prepared in physiological conditions (10 mM sodium phosphate, 150 mM KCl, and 2 mM MgCl₂) and incubation was done at 37 °C for 16 h in thermal cycler (Bio-Rad, USA). The samples were then separated on non-denaturing 8% polyacrylamide gel at 120 V for 35 min. The bound and unbound fractions of the miR-155 were stained with SYBR gold (Invitrogen, USA) and visualized using the Gel-Doc EZ imager (Bio-Rad, USA).

Thermal Melting Analysis: Both the regular PNA-155 and γ PNA-155 were incubated with the target miR-155 in physiological conditions at 1:1 ratio. The samples were subjected to a temperature ramp from 95 to 25 °C and 25 to 95 °C at 1 °C per min. The absorbance was recorded every 0.5 °C increase in temperature at 260 nm using UV-vis spectrophotometer.

Characterization of PNA SA and NA: DLS technique was used to determine the size and PDI of the PNA based SA and NA. PNA NAs were diluted in 0.2 micron filtered purified water to a 10 \times dilution and hydrodynamic size was measured using the Nano-ZS from Malvern

Panalytical (USA). The size and PDI of PNA-155 or γ PNA-155 SA was also determined at the same concentration as 10 \times dilution of PNA NA using purified water as a diluent. The measurements were performed at 25 °C using 1.33 as refractive index. The surface charge of PNA SA and NA was determined by measuring the zeta potential at 25 °C utilizing laser Doppler micro-electrophoresis technique.

Transmission Electron Microscopy: The γ PNA-155 and PNA-155 based SA and NA were stained with 1% w/v uranyl acetate at RT for 5 min on carbon grid (400 mesh copper) followed by washing with water. The samples were allowed to dry for 10 min followed by imaging using FEI Technai at 80 kV voltage.

Cell Culture: HeLa cells were cultured in 10 cm petridishes using EMEM media supplemented with 10% v/v FBS and 1% v/v Pen-Strep. The HeLa cells were passaged as they reached 90% confluency. U2932 and PBMC cells were cultured in T-75 flasks using RPMI media supplemented with 10% v/v FBS and 1% v/v Pen-Strep. PBMC cells were used within 48 h of thawing the cells. The cells were kept in the incubator at 37 °C and 5% CO₂.

Cellular Uptake Studies: The uptake of γ PNA-155 and γ PNA-155 NA were studied in HeLa as well as U2932 cells. The cellular uptake was visualized using confocal microscopy and quantification was confirmed using flow cytometry analysis.

Confocal Microscopy: 8-well chamber slides were used to grow the HeLa cells (50 000 cells per well). The HeLa cells were then treated with the γ PNA-155 and γ PNA-155 NA at the PNA equivalent doses of 0.5, 1, and 2 μ m. After 24 h of treatment, PBS was used to wash the extracellular γ PNA-155 and γ PNA-155 NA followed by staining of the nucleus with hoechst dye 33342 (R37605, Thermo Fisher, USA). The cells were washed again with PBS and suspended in the CO₂ independent media (Gibco, USA). The live cells were immediately imaged at 60 \times on the Nikon A1R microscope.

24 well plates were used to grow 100 000 U2932 cells per well. PNA equivalent doses of γ PNA-155 and γ PNA-155 NA at 0.5, 1, and 2 μ m were added to the wells. 24 h post-treatment, cells were washed with PBS and nucleus was stained with the hoechst dye for 25–30 min. Cells were washed again with PBS and final pellet was resuspended in 15 μ L of growth media. The resuspended cell pellet was then transferred to the glass slide and covered with the 1 mm coverslip. The samples were imaged right away to visualize the cellular uptake in U2932 cells.

Flow Cytometry: To quantify the uptake of γ PNA-155 and γ PNA-155 NA, 24 well plates were used to grow HeLa and U2932 cells. γ PNA-155 and γ PNA-155 NA were added to the cells at the PNA equivalent doses of 0.5, 1, and 2 μ m. After 24 h, HeLa cells were washed twice with PBS and trypsinized by adding 100 μ L of 0.25% trypsin (Gibco, USA) followed by incubation at 37 °C and 5% CO₂ for 5–10 min. The HeLa cells were then collected in the 1.5 mL tubes by centrifuging (2000 RPM) at 4 °C. The treated and untreated U2932 cells (suspended) were directly transferred to the 1.5 mL tube and centrifuged at 4 °C. The U2932 cell pellet was washed with PBS and centrifuged again. The washed U2932 cells were resuspended in 300 μ L of PBS. The cell suspension of both HeLa and U2932 were transferred to the FACS tubes and maintained on ice. Without any delay, samples were evaluated using Fortessa cell analyzer (BD Biosciences, USA) to quantify the uptake of γ PNA-155 and γ PNA-155 NA.

Endocytosis Inhibition Study: The uptake of γ PNA-155 and γ PNA-155 NA was also studied at 4 °C (low temperature) in HeLa cells. HeLa cell lines were pre-incubated at 4 °C for 1 h followed by treatment with γ PNA-155 and γ PNA-155 NA. After 2 h, treated and untreated HeLa cells were washed, trypsinized, and transferred to the FACS tubes. The uptake was quantified using Fortessa X-20 cell analyzer (BD Biosciences, USA). Further, different endocytic pathways were inhibited using CPZ at 10 μ g mL⁻¹, genistein at 200 μ M, and amiloride at 1 mM in HeLa cells for 1 h (pre-treatment) at 37 °C. γ PNA-155 and γ PNA-155 NA were then added to the pre-treated HeLa cells. After 2 h, HeLa cells were trypsinized and transferred to the FACS tube for flow cytometry analysis. For confocal microscopy, the nucleus of treated HeLa cells was stained with hoechst dye and images were taken using a Nikon A1R confocal microscope.

Quantitative Real Time Polymerase Chain Reaction: 12 well plates were used to seed 200 000 U2932 cells per well. γ PNA-155 and γ PNA-155 NA were used at the equivalent dose of 0.5 and 1 μ m. After 48 h of treatment, cells were transferred to the 1.5 mL tube and washed with PBS once. The total RNA was extracted from the treated and untreated U2932 cell pellets using Qiagen RNAeasy kit (Germany). cDNA was synthesized using the target specific primers (miR-155 assay ID: 467534_mat and U6 assay ID: 001973) and following the conditions recommended in high capacity cDNA reverse transcription kit from applied biosystems (USA). The cDNA was then amplified using target specific primers and universal master mix II (Applied Biosystems, USA) under the recommended conditions using CFX connect RT-PCR detection system (Bio-Rad, USA). U6 snRNA was used as the reference gene for miR-155 quantification. The TaqMan gene expression assays for *PTEN* (Hs02621230_s1), *FOXO3A* (Hs00818121_m1), *CSF1R* (Hs00911250_m1), and *JARID2* (Hs01004467_m1) were used for PCR. *GAPDH* (Hs02786624_g1) was used as the reference gene for downstream mRNA target evaluation.

Cell Viability Assay: The viability of PBMC and U2932 cells after treatment with γ PNA-155 and γ PNA-155 NA was determined using CellTiter-Glo luminescence-based assay (G7570, Promega, USA). 96 well plate was used to seed 20 000 PBMC and U2932 cells per well. γ PNA-155 and γ PNA-155 NA were added at indicated PNA equivalent doses. After 48 h, cells were incubated at RT for 30 min and 100 μ L of CellTiter-Glo reagent was added. The plate was kept on a shaker for 30 s and kept at RT for 10 min. The luminescence signal was then captured using the Tecan plate reader.

Apoptosis Assay: Annexin V apoptosis detection kit (BD Biosciences, USA) was used to determine the apoptosis in U2932 cells. γ PNA-155 and γ PNA-155 NA were added at 0.5 μ m PNA equivalent dose. After 48 h, cells were collected in the 1.5 mL tubes and centrifuged at 2000 RPM for 3 min at 4 °C. The treated and untreated U2932 cells were counted using the cell counter (Bio-Rad, USA). U2932 cells (100 000) were then transferred to the FACS tubes and stained with 10 μ L of each 7-AAD and Annexin V PE. The cells were incubated in dark for 15 min followed by addition of 400 μ L Annexin V binding buffer to the FACS tubes. The samples were analyzed using the Fortessa Cell analyzer (BS Bioscience, USA) using unstained cells, only 7-AAD stained and Annexin V stained cells as controls. The results were analyzed using flowjo analysis software.

Small-Angle Neutron Scattering: γ PNA-155 NA was formulated using D₂O and ethanol injection method to obtain 5 mg mL⁻¹ concentration. The SANS setup at National Institute of Science and Technology (NIST) Center for Neutron Research (NCNR, Gaithersburg, MD). The average wavelength, λ of 6 Å was used with a spread of 12.5%. This yielded a q range [$q \equiv \frac{4\pi}{\lambda} \sin\left(\frac{\theta}{2}\right)$, where θ is the scattering angle] from 0.001 to 0.4 Å⁻¹. The front and middle detectors were used for low and high q data collection, respectively. The 2D raw data were corrected by the detector sensitivity, background, scattering and transmission of empty cells, and sample transmission. The corrected data were then circularly averaged, yielding 1D profiles and the intensity was put on the absolute scale using the measured incident beam flux. The data reduction package was provided by NIST using the IGOR macros with IGOR Pro software. The SANS data were analyzed by using SASView 4.2.2.

Small-Angle X-Ray Scattering: SAXS experiments were performed with the 16ID-LiX Beamline at National Synchrotron Light Source II at the Brookhaven National Laboratory (Upton, NY). Samples were loaded and measured with the high throughput flow cell solution scattering setup with an X-ray energy of 13.5 keV. The scattering images were acquired with 1 s of exposure time for twice and averaged to yield the 2D raw data, which were then circularly averaged and reduced to 1D profiles as a function of scattering vector, SAXS intensity was presented as a function of scattering vector, q varying from 0.005 to 2.5 Å⁻¹. To reduce the intensity of hydrogen bond, transmission correction and background subtraction was done at $q \approx 2.0$ Å⁻¹. The SAXS data were also analyzed by using SASView 4.2.2.

Supporting Information

Supporting Information is available from the Wiley Online Library or from the author.

Acknowledgements

Access to SANS was provided by the Center for High Resolution Neutron Scattering, a partnership between the National Institute of Standards and Technology and the National Science Foundation under Agreement no: DMR-2010792. Certain commercial equipment, instruments, materials, suppliers, or software are identified in this paper to foster understanding. Such identification does not imply recommendation or endorsement by the National Institute of Standards and Technology, nor does it imply that the materials or equipment identified are necessarily the best available for the purpose. The authors would like to thank Dr. Lin Yang for his help with collecting the SAXS data at 16-ID LiX beamline of the National Synchrotron Light Source II, a U.S. Department of Energy (DOE) Office of Science User Facility operated for the DOE Office of Science by Brookhaven National Laboratory under Contract no. DE-SC0012704. This work was supported by Hood Foundation award and NIH (R01) (CA241194-01A1 and HL147028-01A1) grant provided to R.B. The Center for BioMolecular Structure (CBMS) is primarily supported by the National Institutes of Health, National Institute of General Medical Sciences (NIGMS) through a Center Core P30 Grant (P30GM133893), and by the DOE Office of Biological and Environmental Research (KP1607011). The small-angle neutron and X-ray scattering analysis benefited from the use of the SasView application, originally developed under NSF Award DMR-0520547. SasView also contains code developed with funding from the EU Horizon 2020 programme under the SINE2020 project Grant No 654000.

Conflict of Interest

The authors declare no conflict of interest.

Data Availability Statement

The data that support the findings of this study are available from the corresponding author upon reasonable request.

Keywords

gamma peptide nucleic acids, micro-RNA-155, nano-assemblies, peptide nucleic acid amphiphiles, self-assembly

Received: September 21, 2021

Revised: October 23, 2021

Published online: November 5, 2021

- [1] P. E. Nielsen, M. Egholm, R. H. Berg, O. Buchardt, *Science* **1991**, 254, 1497.
 [2] P. Wittung, P. E. Nielsen, O. Buchardt, M. Egholm, B. Norden, *Nature* **1994**, 368, 561.
 [3] V. V. Demidov, V. N. Potaman, M. D. Frank-Kamenetskii, M. Egholm, O. Buchardt, S. H. Sonnichsen, P. E. Nielsen, *Biochem. Pharmacol.* **1994**, 48, 1310.
 [4] M. Egholm, O. Buchardt, L. Christensen, C. Behrens, S. M. Freier, D. A. Driver, R. H. Berg, S. K. Kim, B. Norden, P. E. Nielsen, *Nature* **1993**, 365, 566.

- [5] a) R. Bahal, N. Ali McNeer, E. Quijano, Y. Liu, P. Sulkowski, A. Turchick, Y. C. Lu, D. C. Bhunia, A. Manna, D. L. Greiner, M. A. Brehm, C. J. Cheng, F. Lopez-Giraldez, A. Ricciardi, J. Beloor, D. S. Krause, P. Kumar, P. G. Gallagher, D. T. Braddock, W. Mark Saltzman, D. H. Ly, P. M. Glazer, *Nat. Commun.* **2016**, 7, 13304; b) R. Bahal, E. Quijano, N. A. McNeer, Y. Liu, D. C. Bhunia, F. Lopez-Giraldez, R. J. Fields, W. M. Saltzman, D. H. Ly, P. M. Glazer, *Curr. Gene Ther.* **2014**, 14, 331; c) A. S. Ricciardi, R. Bahal, J. S. Farrelly, E. Quijano, A. H. Bianchi, V. L. Luks, R. Putman, F. Lopez-Giraldez, S. Coskun, E. Song, Y. Liu, W. C. Hsieh, D. H. Ly, D. H. Stitelman, P. M. Glazer, W. M. Saltzman, *Nat. Commun.* **2018**, 9, 2481.
 [6] a) I. A. Babar, C. J. Cheng, C. J. Booth, X. Liang, J. B. Weidhaas, W. M. Saltzman, F. J. Slack, *Proc. Natl. Acad. Sci. USA* **2012**, 109, E1695; b) C. J. Cheng, R. Bahal, I. A. Babar, Z. Pincus, F. Barrera, C. Liu, A. Svoronos, D. T. Braddock, P. M. Glazer, D. M. Engelman, W. M. Saltzman, F. J. Slack, *Nature* **2015**, 518, 107; c) S. Malik, J. Lim, F. J. Slack, D. T. Braddock, R. Bahal, *J. Controlled Release* **2020**, 327, 406; d) A. Tahmasbi Rad, S. Malik, L. Yang, T. K. Oberoi-Khanuja, M. P. Nieh, R. Bahal, *Nanoscale* **2019**, 11, 12517.
 [7] R. D'Agata, M. C. Giuffrida, G. Spoto, *Molecules* **2017**, 22, 1951.
 [8] S. Galbiati, B. Foglieni, M. Travi, C. Curcio, G. Restagno, L. Sbaiz, M. Smid, F. Pasi, A. Ferrari, M. Ferrari, L. Cremonesi, *Haematologica* **2008**, 93, 610.
 [9] A. Singer, S. Rapireddy, D. H. Ly, A. Meller, *Nano Lett.* **2012**, 12, 1722.
 [10] E. Quijano, R. Bahal, A. Ricciardi, W. M. Saltzman, P. M. Glazer, *Yale J. Biol. Med.* **2017**, 90, 583.
 [11] B. M. McMahon, D. Mays, J. Lipsky, J. A. Stewart, A. Fauq, E. Richelson, *Antisense Nucleic Acid Drug Dev.* **2002**, 12, 65.
 [12] J. J. Turner, G. D. Ivanova, B. Verbeure, D. Williams, A. A. Arzumanov, S. Abes, B. Lebleu, M. J. Gait, *Nucleic Acids Res.* **2005**, 33, 6837.
 [13] P. Bhingardev, B. R. Madhanagopal, H. Naick, P. Jain, M. Manoharan, K. Ganesh, *J. Org. Chem.* **2020**, 85, 8812.
 [14] a) S. Malik, B. Asmara, Z. Moscato, J. K. Mukker, R. Bahal, *Curr. Pharm. Des.* **2018**, 24, 5164; b) S. Volpi, U. Cancelli, M. Neri, R. Corradini, *Pharmaceuticals* **2020**, 14, 14.
 [15] O. Berger, E. Gazit, *Biopolymers* **2017**, 108, 10.
 [16] P. Katyal, M. Meleties, J. K. Montclare, *ACS Biomater. Sci. Eng.* **2019**, 5, 4132.
 [17] F. Zhang, J. Nangreave, Y. Liu, H. Yan, *J. Am. Chem. Soc.* **2014**, 136, 11198.
 [18] J. P. Vernille, L. C. Kovell, J. W. Schneider, *Bioconjugate Chem.* **2004**, 15, 1314.
 [19] M. O. Guler, J. K. Pokorski, D. H. Appella, S. I. Stupp, *Bioconjugate Chem.* **2005**, 16, 501.
 [20] P. S. Lukeman, A. C. Mittal, N. C. Seeman, *Chem. Commun.* **2004**, 1964.
 [21] O. Berger, L. Adler-Abramovich, M. Levy-Sakin, A. Grunwald, Y. Liebes-Peer, M. Bachar, L. Buzhansky, E. Mossou, V. T. Forsyth, T. Schwartz, Y. Ebenstein, F. Frolov, L. J. Shimon, F. Patolsky, E. Gazit, *Nat. Nanotechnol.* **2015**, 10, 353.
 [22] a) H. Cui, M. J. Webber, S. I. Stupp, *Biopolymers* **2010**, 94, 1; b) J. D. Hartgerink, E. Beniash, S. I. Stupp, *Proc. Natl. Acad. Sci. USA* **2002**, 99, 5133; c) X. Zhao, F. Pan, H. Xu, M. Yaseen, H. Shan, C. A. Hauser, S. Zhang, J. R. Lu, *Chem. Soc. Rev.* **2010**, 39, 3480.
 [23] C. Lau, R. Bitton, H. Bianco-Peled, D. G. Schultz, D. J. Cookson, S. T. Grosser, J. W. Schneider, *J. Phys. Chem. B* **2006**, 110, 9027.
 [24] C. R. James, A. M. Rush, T. Insley, L. Vukovic, L. Adamiak, P. Kral, N. C. Gianneschi, *J. Am. Chem. Soc.* **2014**, 136, 11216.
 [25] A. Manicardi, R. Corradini, *Artif. DNA PNA XNA* **2014**, 5, e1131801.
 [26] a) A. Dragulescu-Andrasi, S. Rapireddy, B. M. Frezza, C. Gayathri, R. R. Gil, D. H. Ly, *J. Am. Chem. Soc.* **2006**, 128, 10258; b) B. Sahu,

- I. Sacui, S. Rapireddy, K. J. Zanotti, R. Bahal, B. A. Armitage, D. H. Ly, *J. Org. Chem.* **2011**, *76*, 5614.
- [27] I. Sacui, W. C. Hsieh, A. Manna, B. Sahu, D. H. Ly, *J. Am. Chem. Soc.* **2015**, *137*, 8603.
- [28] S. Kumar, A. Pearse, Y. Liu, R. E. Taylor, *Nat. Commun.* **2020**, *11*, 2960.
- [29] A. Esquela-Kerscher, F. J. Slack, *Nat. Rev. Cancer* **2006**, *6*, 259.
- [30] a) S. Malik, F. J. Slack, R. Bahal, *MethodsX* **2020**, *7*, 101115; b) L. Christensen, R. Fitzpatrick, B. Gildea, K. H. Petersen, H. F. Hansen, T. Koch, M. Egholm, O. Buchardt, P. E. Nielsen, J. Coull, R. H. Berg, *J. Pept. Sci.* **1995**, *1*, 175.
- [31] P. S. Eis, W. Tam, L. Sun, A. Chadburn, Z. Li, M. F. Gomez, E. Lund, J. E. Dahlberg, *Proc. Natl. Acad. Sci. USA* **2005**, *102*, 3627.
- [32] C. Jaafar-Maalej, R. Diab, V. Andrieu, A. Elaissari, H. Fessi, *J. Liposome Res.* **2010**, *20*, 228.
- [33] a) S. Batzri, E. D. Korn, *Biochim. Biophys. Acta* **1973**, *298*, 1015; b) S. S. Marques, I. I. Ramos, S. R. Fernandes, L. Barreiros, S. A. C. Lima, S. Reis, M. R. M. Domingues, M. A. Segundo, *Molecules* **2020**, *25*, 1879.
- [34] S. Franze, F. Selmin, E. Samaritani, P. Minghetti, F. Cilurzo, *Pharmaceutics* **2018**, *10*, 139.
- [35] W. Abdelwahed, G. Degobert, S. Stainmesse, H. Fessi, *Adv. Drug Delivery Rev.* **2006**, *58*, 1688.
- [36] U. Koppelhus, S. K. Awasthi, V. Zachar, H. U. Holst, P. Ebbesen, P. E. Nielsen, *Antisense Nucleic Acid Drug Dev.* **2002**, *12*, 51.
- [37] S. Engelberg, J. Modrejewski, J. G. Walter, Y. D. Livney, Y. G. Assaraf, *Oncotarget* **2018**, *9*, 20993.
- [38] a) A. Tahmasbi Rad, C. W. Chen, W. Aresh, Y. Xia, P. S. Lai, M. P. Nieh, *ACS Appl. Mater. Interfaces* **2019**, *11*, 10505; b) W. Aresh, Y. Liu, J. Sine, D. Thayer, A. Puri, Y. Huang, Y. Wang, M. P. Nieh, *J. Biomed. Nanotechnol.* **2016**, *12*, 1852.
- [39] K. L. Goldenthal, I. Pastan, M. C. Willingham, *Exp. Cell Res.* **1984**, *152*, 558.
- [40] A. Sofer, A. H. Futerman, *J. Biol. Chem.* **1995**, *270*, 12117.
- [41] I. R. Nabi, P. U. Le, *J. Cell Biol.* **2003**, *161*, 673.
- [42] M. Koivusalo, C. Welch, H. Hayashi, C. C. Scott, M. Kim, T. Alexander, N. Touret, K. M. Hahn, S. Grinstein, *J. Cell Biol.* **2010**, *188*, 547.
- [43] a) C. Cordier, F. Boutimah, M. Bourdeloux, F. Dupuy, E. Met, P. Alberti, F. Loll, G. Chassaing, F. Burlina, T. E. Saison-Behmoaras, *PLoS One* **2014**, *9*, e104999; b) M. Ghavami, T. Shiraishi, P. E. Nielsen, *Biomolecules* **2019**, *9*, 554.
- [44] G. Hartmann, *Adv. Immunol.* **2017**, *133*, 121.
- [45] R. Kedmi, N. Ben-Arie, D. Peer, *Biomaterials* **2010**, *31*, 6867.
- [46] L. Jansky, P. Reymanova, J. Kopecky, *Physiol. Res.* **2003**, *52*, 593.
- [47] J. Kluiver, S. Poppema, D. de Jong, T. Blokzijl, G. Harms, S. Jacobs, B. J. Kroesen, A. van den Berg, *J. Pathol.* **2005**, *207*, 243.
- [48] M. Metzler, M. Wilda, K. Busch, S. Viehmann, A. Borkhardt, *Genes, Chromosomes Cancer* **2004**, *39*, 167.
- [49] P. de Diesbach, F. N'Kuli, C. Berens, E. Sonveaux, M. Monsigny, A. C. Roche, P. J. Courtoy, *Nucleic Acids Res.* **2002**, *30*, 1512.
- [50] E. Anastasiadou, A. G. Seto, X. Beatty, M. Hermreck, M. E. Gilles, D. Stroopinsky, L. C. Pinter-Brown, L. Pestano, C. Marchese, D. Avigan, P. Trivedi, D. M. Escolar, A. L. Jackson, F. J. Slack, *Clin. Cancer Res.* **2021**, *27*, 1139.
- [51] a) I. M. Pedersen, D. Otero, E. Kao, A. V. Miletic, C. Hother, E. Ralfkiaer, R. C. Rickert, K. Gronbaek, M. David, *EMBO Mol. Med.* **2009**, *1*, 288; b) S. Costinean, N. Zanesi, Y. Pekarsky, E. Tili, S. Volinia, N. Heerema, C. M. Croce, *Proc. Natl. Acad. Sci. USA* **2006**, *103*, 7024.
- [52] A. Gupta, R. Bahal, M. Gupta, P. M. Glazer, W. M. Saltzman, *J. Controlled Release* **2016**, *240*, 302.
- [53] T. Shiraishi, P. E. Nielsen, *Methods Mol. Biol.* **2014**, *1050*, 193.
- [54] A. Gupta, E. Quijano, Y. Liu, R. Bahal, S. E. Scanlon, E. Song, W. C. Hsieh, D. E. Braddock, D. H. Ly, W. M. Saltzman, P. M. Glazer, *Mol. Ther.–Nucleic Acids* **2017**, *9*, 111.
- [55] S. Kumar, I. Dhami, S. A. Thadke, D. H. Ly, R. E. Taylor, *Biopolymers* **2021**, e23463.
- [56] S. Kumar, Y. Liu, R. E. Taylor, *J. Vis. Exp.* **2020**, *160*, e61351.